Steel and Composite Structures, Vol. 1, No. 3 (2001) 313-328
DOI: http://dx.doi.org/10.12989/scs.2001.1.3.313

Confinement evaluation of concrete-filled box-shaped steel columns

K.A.S. Susantha†, Hanbin Ge‡ and Tsutomu Usami‡†

Department of Civil Engineering, Nagoya University, Chikusa-ku, Nagoya 464-8603, Japan

Abstract. This paper presents a three-dimensional finite element analysis methodology for a quantitative evaluation of confinement in concrete-filled box-shaped unstiffened steel columns. The confinement effects of concrete in non-circular sections can be assessed in terms of maximum average lateral pressure. A brief review of a previous method adopted for the same purpose is also presented. The previous method is based on a two-dimensional finite element analysis method involving a concrete-steel interaction model. In both the present and previous methods, average lateral pressure on concrete is computed by means of the interaction forces present at the concrete-steel interface. Subsequently, the strength enhancement of confined concrete is empirically related to the maximum average lateral pressure. The results of the former and latter methods are then compared. It is found that the results of both methods are compatible in terms of confined concrete strengths, although the interaction model yields a somewhat overestimated estimation of confinement than those of the present method when relatively high strength concrete is used. Furthermore, the confinement in rectangular-shaped sections is investigated and the reliability of previously adopted simplifications in such cases is discussed.

Key words: concrete-filled tubes; box-shaped CFT columns; confinement; confined concrete; concrete-steel interface; composite action.

1. Introduction

The strength enhancement in excess of uniaxial strength and the deformation improvement of concrete can be observed when concrete is subjected to triaxial compressive stress states. Common examples of triaxially loaded concrete can be seen in hoop-reinforced concrete columns, concrete-filled tubes (CFTs), pipe piles and mass concrete structures. Among these, the concrete-filled steel columns are now the focus of attention in regions of high seismic activity. This is due to their excellent earthquake resisting characteristics such as their high ductility and enhanced strength. Even though CFTs are widely applied in engineering structures, the exact behaviour of confined concrete in such structures is complex and not yet well understood. On the other hand, the behaviour of confined concrete in filled-in tubes has been the topic of many past investigations by means of experimental and analytical approaches (e.g., Han *et al*. 2001, Susantha *et al*. 2001, Brauns 1999, Kvedaras and Sapalas 1999, Schneider 1998, Watanabe *et al*. 1997, Tang *et al*. 1996, Ge and Usami 1994, 1992, Baba *et al*. 1995, Tomii *et al*. 1988, Tomii *et al*. 1979a, 1979b, Tomii *et al*. 1977, etc.). In several of these studies, the

†Graduate Student
‡Associate Professor
‡†Professor

amount of confinement has then been represented through an exclusive parameter, which has been used to define the peak point of confined concrete (Han *et al*. 2001, Susantha *et al*. 2001, Tang *et al*. 1996). The concrete mechanical model, as described in Han *et al.* (2001), includes a confinement factor which to some extent represents the composite action between steel and concrete. The strengths and cross sectional areas of steel and concrete are used to define this factor. In a previous work by Susantha *et al.* (2001), the confinement effects on concrete strength and post-peak behaviour were examined extensively using an analytical approach in conjunction with some experimental results. A concrete-steel interaction model was used to determine the maximum average lateral pressure, which is a key index in that it represents the amount of confinement available at the peak load of the CFT columns. A brief review of this procedure including the definition of maximum average lateral pressure will be presented below (section 2). Tang *et al*. (1996) proposed an empirical parameter to determine the lateral pressure on confined concrete at the peak load of circular-shaped columns. This parameter was defined by using the geometrical and material properties of sections. In the works by Susantha *et al*. (2001) and Tang *et al*. (1996), the lateral pressure is correlated to the confined concrete strength through an empirical equation. The model proposed by Watanabe *et al.* (1997) includes the confinement effect as a function of width-to-thickness ratio. However, no direct confinement assessment has been done in this study. Meanwhile, it seems that the quantitative examination of lateral pressure on concrete by exclusively experimental means is a complex and difficult task. On the other hand, analytical approaches are found to be a good alternative in overcoming such difficulties.

This paper is mainly concerned with the confinement evaluation of concrete in box-shaped steel columns using a 3-dimensional nonlinear finite element analysis. On top of that, an empirical equation, previously proposed by the authors (Susantha *et al*. 2001) in the determination of maximum average lateral pressure in box section columns, is verified. The interaction of the concrete-steel interface is further examined at various axial strain levels in order to clarify the actual behaviour of composite materials. The effect of breadth-to-width ratio on confinement efficiency is also investigated with a view to assessing the previously adopted simplifications in the case of rectangular-shaped columns.

2. Summary of concrete-steel interaction model

This section explains a concrete-steel interaction model previously proposed by Susantha *et al*. (2001) for determining the maximum average lateral pressure of box-shaped concrete-filled steel tubes as this is the same objective for the present approach. The maximum average lateral pressure in a square-shaped CFT column, which is presumed to occur at peak axial load, is determined by using an interaction model as shown in Fig. 1(a). The confinement along the height of a column is assumed to be uniform, hence one unit length of column can be considered for analysis, although, this assumption is not exact because lateral pressures around the loading edges are larger than those for the rest of the columns. This is due to the lateral restraints at the loading edges. Thus, the uniform lateral pressure assumption implies that the loading edges are free to move in a lateral direction. The concrete is discretized into a number of segments bounded by the lines joining the center point of the model and mid points of adjacent steel beam elements as shown in Fig. 1(b). Each of these segments is represented by an axial compressive truss element with an equal stiffness of corresponding triangular concrete segments. Lateral steel is also represented by a number of beam-column elements. A similar type of model has been employed by Nishiyama *et al*. (1997) and Assa *et al.* (2001) for lateral pressure evaluations of reinforced concrete columns. The basic difference between Nishiyama’s method and the

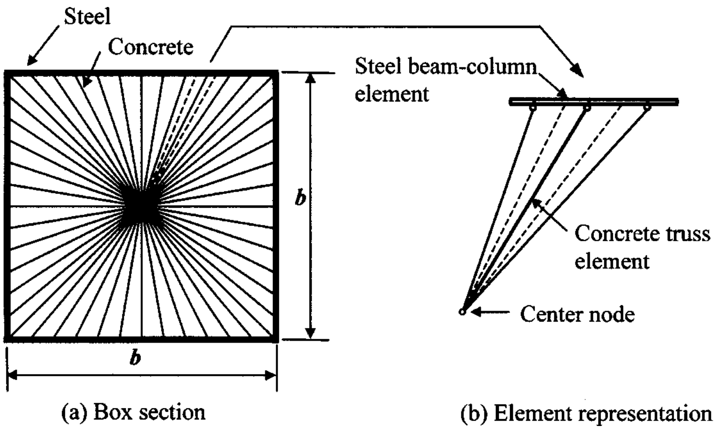

Fig. 1 Interaction model for concrete-filled box section

one being explained here is that the latter assigns a newly defined complete concrete stress-strain relation to be used in truss elements. As a result, the maximum average lateral pressure can be directly obtained from this method. Here, for a pre-assumed uniform lateral strain, corresponding displacements of each of the truss elements are computed and are applied incrementally at each node of the concrete bar elements at the center of the model. This leads to an expansion of the outer steel cage since the steel elements are laterally pushed out by the concrete bar elements. At the end of each load increment, the average lateral stress, f_r^*, and the average lateral strain, ε_r^*, are calculated. The stress f_r^* is computed by summing up all the normal components of reaction forces as facing each side and dividing by the total area that they are acting upon. Then, the maximum value of f_r^* denoted by f_{rp}^*, can be easily obtained. In a triaxial stress state, the uniaxial compressive strength can be given by:

$$f'_{cc} = f'_c + m f_{rp} \tag{1}$$

where f_{rp} is the maximum radial pressure on concrete and m is an empirical coefficient. In the past many experimental studies have tried to determine a value for m. From those it has been found that for normal strength concrete, m is in the range of 4 to 6 (Sugupta and Mendis 1995). Gardner and Jacobson (1967) proposed a value of 4.0 for coefficient m. In this study, m is assumed to be 4.0. A constant strength reduction factor of 0.85 is introduced for unconfined concrete strength, f'_c, for design purposes. The reasons for such a reduction in unconfined concrete strength are: (a) the strength differences between actual columns and test cylinders due to geometry and load application method; and (b) variation in concrete strength along the column length. A review of strength reduction factors for unconfined concrete can be found in a paper by El-Tawil *et al.* (1999) where they used a constant reduction factor of 0.85 for their composite column design studies. From these, confined concrete strength, f'_{cc}, is given by the following equation, which is directly deduced from Eq. (1):

$$f'_{cc} = 0.85 f_c' + 4.0 f_{rp} \tag{2}$$

The maximum average lateral pressure, f_{rp}^*, is then substituted for f_{rp} in Eq. (2) in the case of non-circular section columns.

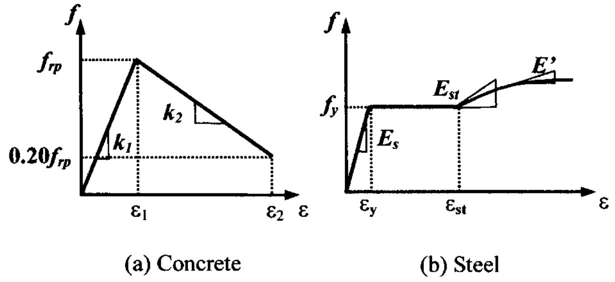

Fig. 2 Material properties for concrete-steel interaction model

2.1. Material models for the concrete-steel interaction model

The concrete stress-strain relation to be employed in the concrete bar elements of the interaction model had to be specifically established. This was done by means of the lateral stress-strain relationship of circular columns. The resulting concrete model to be employed in the interaction model is shown in Fig. 2(a). The parameters appearing in Fig. 2(a) were determined by modifying the expressions proposed by Tang *et al*. (1996) for circular-shaped columns. For example, f_{rp}, that is the maximum lateral pressure on circular tubes, has been utilized to determine the strength of concrete in a lateral direction. If the concrete-steel interaction model is employed for circular-shaped sections, then the strength of concrete bar elements should be equal to f_{rp}, which is given by (Tang *et al*. 1996)

$$f_{rp} = \beta\frac{2t}{(D-2t)} f_y \tag{3}$$

where f_y, t and D denote the yield stress of steel, the thickness and the outer diameter of the tube, respectively, and β is an empirical parameter, which is determined using the changes in the Poisson's ratios of steel subjected to monotonic axial loading. The strength of concrete elements in the interaction model of box-shaped columns is then determined by modifying Eq. (3). That is, the diameter D is replaced by the outer dimension of box section, b, and the parameter β is determined by the difference between υ_e and υ_s at the maximum strength point where, υ_e and υ_s are the Poisson's ratios of steel tubes with and without filled-in concrete, respectively. The parameter υ_e is given by

$$\upsilon_e = 0.2312 + 0.3582\upsilon_e' - 0.1524(f_c'/f_y) + 4.843\upsilon_e'(f_c'/f_y) - 9.169(f_c'/f_y)^2 \tag{4}$$

where

$$\upsilon_e' = 0.881\times10^{-6}(D_{eq}/t)^3 - 2.58\times10^{-4}(D_{eq}/t)^2 + 1.953\times10^{-2}(D_{eq}/t) + 0.4011 \tag{5}$$

It should be mentioned here that Eq. (5) was deduced by replacing parameter D as it appeared in the original equations proposed by Tang *et al*. (1996) by parameter D_{eq} which is obtained by equating the area of the box section to its equivalent circular-shaped section ($=2b/\sqrt{\pi}$ for square section with a side length of b). The falling branch slope, k_2, is calibrated using the test results of Watanabe *et al*. (1997). Consequently, k_1 and k_2 are given by

$$k_1 = \frac{2t}{(D_{ed} - 2t)} E_s \tag{6}$$

$$k_2 = 2744\left[\left(\frac{D_{ed}}{t}\right)\left(\frac{f_c'}{f_y}\right) - 266\left(\frac{D_{ed}}{t}\right)\left(\frac{f_c'}{f_y}\right)\right]^2 - 7637 \le 0 \tag{7}$$

Fig. 2(b) shows the steel material model adopted in the interaction model. For steel material parameters, yield stress, f_y, the elastic modulus, E_s, and the Poisson's ratio, ν, for each specimen are taken as the values reported in Watanabe *et al*. (1997). The strain hardening modulus, E', is given by

$$E' = E_{st}\exp\left(-\xi\frac{\varepsilon - \varepsilon_{st}}{\varepsilon_y}\right) \tag{8}$$

where, the values for initial strain hardening modulus, E_{st}, the strain at the onset of strain hardening, ε_{st}, and yield strain, ε_y, are assumed to be the same for a mild steel of the kind SS400 (Usami and Ge 1998).

2.2. Expression for the maximum lateral pressure

Using the foregoing procedure, extensive parametric analyses have been conducted and a general expression for the maximum average lateral pressure has been proposed. The results of such analyses conducted on the square-shaped sections are shown in Fig. 3. Consequently, an empirical equation has been established to compute f_{rp}^* as:

$$f_{rp}^* = -6.5R\frac{f_c'^{1.46}}{f_y} + 0.12 f_c'^{1.03} \tag{9}$$

with

$$R = \frac{b}{t}\sqrt{\frac{12(1-\upsilon^2)}{4\pi^2}}\sqrt{\frac{f_y}{E_s}} \tag{10}$$

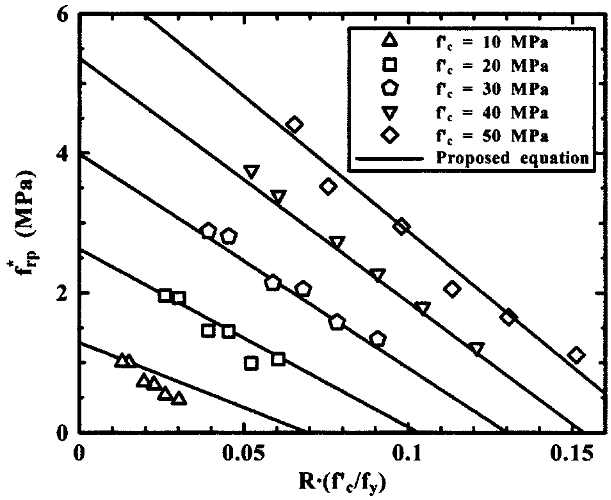

Fig. 3 Maximum average lateral pressure by the interaction model

where R is the width-to-thickness ratio parameter of the component plate (Ge and Usami 1994). Here, b is the flange plate breadth, E_s and υ are respectively the Young's modulus and the Poison's ratio of steel. In this study, the geometry and material parameters are chosen in such a way that the local buckling could be ignored when columns are axially loaded. This is achieved by keeping a certain upper bound, say 0.85, for parameter R based on the expressions proposed for the local buckling strength of plates in CFT columns (Ge and Usami 1994). In the case of rectangular-shaped sections, the same expression as given in Eq. (9) is adopted by defining R corresponding to the plate at the longer side of section. This is a simple assumption which results in conservative predictions.

3. Confinement evaluation by 3-dimensional analysis

As previously mentioned there have only been a few experimental and analytical approaches available for a quantitative assessment of confinement present in CFT columns (e.g., Han *et al*. 2001, Susantha *et al*. 2001, Tang *et al*. 1996). Among them, the one proposed by Susantha *et al.* (2001) was based on a 2-dimensional finite element analysis procedure, and included a set of assumptions to simplify the complexity of the problem. Thus, such simple approaches have to be verified by more accurate analyses or extensive experiments. The experimental approaches suitable for lateral pressure verifications are complicated and costly. Therefore, a comprehensive 3-dimensional (3D) finite element analysis procedure has been adopted to investigate confinement behaviour and to ensure the accuracy of the simplified approach explained in the preceding section. Additionally, the simplifications adopted to deal with the confinement in rectangular-shaped columns are also assessed.

3.1. Analytical model

To evaluate lateral pressure, a column consisting of a relatively small height is selected as shown in Fig. 4. The core concrete is modelled by using 8-node brick elements with three degrees of freedom per node whilst the steel tube is modelled by using 4-node shell elements with six degrees of freedom per node. Only one eighth of the column is modelled because of its symmetry in geometry and loading. The analyses are conducted by using the general purpose finite element analysis program ABAQUS (1998). The concrete-steel interface is modelled using a type of interface element called, the "gap element",

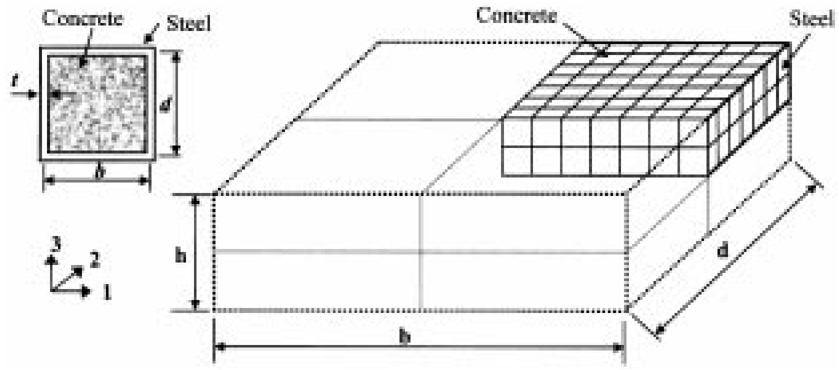

Fig. 4 One-eighth of the column for finite element modelling

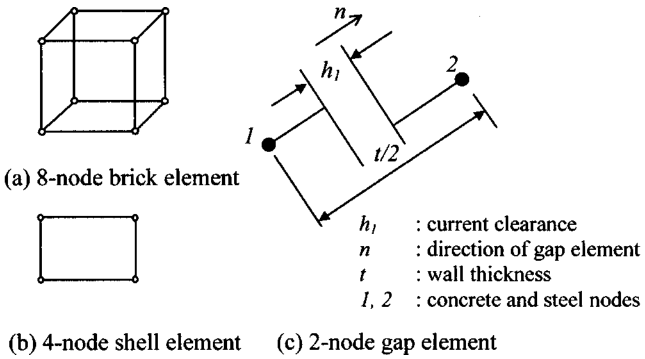

Fig. 5 Types of elements

available in the program. All the outer surface nodes of concrete elements are connected to the adjacent steel nodes through the gap elements. A schematic illustration of such a connection between the concrete and steel tube is shown in Fig. 5(c). Each gap element has two end nodes, and the current clearance between two nodes is defined as

$$h_1 = h_0 + n \cdot (u^2 - u^1) \geq 0 \tag{11}$$

where h_0 is the initial clearance of the two surfaces, n is the direction of the gap element and u^2 and u^1 are the total displacements at nodes 1 and 2, respectively. The behaviour of gap elements is such that when concrete and steel surfaces are in contact, contact forces (gap forces) develop. Whenever the contact is broken (i.e., separation of the two materials) the gap forces become zero. The initial gap clearance, h_0, is set to zero so that the concrete-steel interface is considered to be in contact prior to loading. Frictional forces developed at the interface can be included explicitly through a friction coefficient. For the purpose of this study the friction coefficient is designated as 0.25. The incremental vertical displacements are simultaneously applied to the concrete and steel nodes at the top of the column, and the forces at each gap element are recorded. No lateral constraints are enforced at the top or bottom edges so that the steel tube can expand freely in a lateral direction, as shown in Fig. 6. This is to ensure that the lateral pressure distribution along the column height is

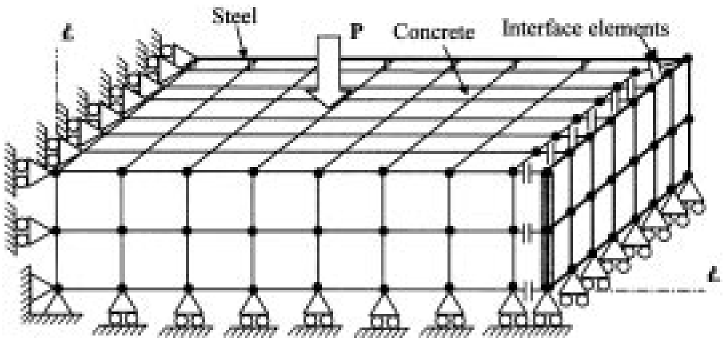

Fig. 6 Analytical model

uniform to a large extent. This also complies with the assumption of uniform lateral pressure made in the interaction model. However, the gap element forces along the height of a column do vary to some extent. Also, it is obvious that the gap element forces across a given section are not uniform in the non-circular shape sections. As a result, the overall effect of gap element forces are to be accounted for in terms of average lateral pressure, f_r, which is defined by

$$f_r = \frac{\sum_{i=1}^{N_t} F_i}{A} \tag{12}$$

where F_i is the force in ith gap element, N_t is the total number of gap elements, and A denotes the total area of concrete-steel interface. It is should be noted that the same kind of averaging concept was used in the previous interaction model too.

3.1.1. Stress-strain models of concrete and steel

The three-dimensional constitutive law of concrete available in the ABAQUS program is employed here for the behaviour of filled-in concrete. This model is applicable in situations where concrete is subjected to an essentially monotonic straining at low confinement pressures (less than four to five times the largest compressive stress that can be carried by the concrete in uniaxial compression). It is well known that the level of confinement in filled-in concrete is relatively low (Schneider 1998, Tomii *et al.* 1977), and so this model is adequate for the present analysis. It consists of an isotropically hardening yield surface when stress is dominantly compressive and an independent "crack detection surface" that determines if a point fails due to cracking. The oriented damaged elasticity concept is used to describe the reversible part of the material's response after cracking failure (ABAQUS Theory Manual 1998). In the absence of uniaxial compressive stress-strain test data, required for the model calibration, a compressive stress-strain relation of unconfined concrete as proposed by Kent and Park (1971) is adopted with slight modifications such as the inclusion of tensile part and the extension of the falling branch up to zero stress, as shown in Fig. 7. Here, the tensile strength of concrete is assumed to be 10 percent of its uniaxial compressive strength. In this model, the strain at the peak stress is assumed to be 0.002, and the expressions for the ascending and descending parts (i.e., OA and AB, respectively) are as shown in the figure. The falling branch is assumed to be a linear, which is decided by the point where

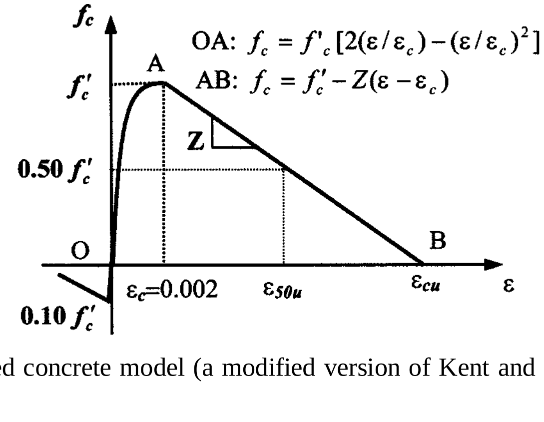

Fig. 7 Unconfined concrete model (a modified version of Kent and Park model 1971)

Table 1 Steel material properties

Parameter	SS400	SM490	SM570
f_y (MPa)	235.0	314.0	450.0
E_s (MPa)	2.06×10^5	2.06×10^5	2.06×10^5
υ	0.30	0.30	0.30
$\varepsilon_{st}/\varepsilon_y$	10	7	3
E_{st}/E_s	1/40	1/30	1/100
ξ	0.06	0.06	0.02

stress has fallen to 50 percent of the maximum stress. The strain, ε_{50u}, at $0.5f'_c$ on the falling branch is given by

$$\varepsilon_{50u} = \frac{3 + 0.002f_c'}{f_c' - 1000} \tag{13}$$

in which f'_c is in psi (Kent and Park 1971).

The same elasto-plastic stress-strain relation as presented in Fig. 2(b) is employed for steel. Three types of steel (SS400, SM490 and SM570) are adopted in the analysis (Ge and Usami 1998). The material parameters for these three types of steel are given in Table 1.

3.1.2. Effects of mesh division and aspect ratio (b/h)

The mesh sensitivity and the effects of the *b/h* ratio on results are investigated in order to establish a proper analytical model. Three cases are considered for the mesh sensitivity checks in such a way that each layer of the model contains 25, 36 and 49 concrete elements (i.e., the total number of elements in one layer, *N*, including steel elements, being 35, 48 and 63). The analyses are conducted for three values of *b/h* ratios (3.5, 10 and 15) and the maximum average lateral pressure, f_{rp}, for each case is computed. The results are shown in Fig. 8 where the effects of the mesh size is not so significant. However, to facilitate the smooth tracing of lateral pressure distribution across a section, the third case (i.e., $N = 63$) can be seen as the most appropriate. Then, the effect of the *b/h* ratio is investigated by

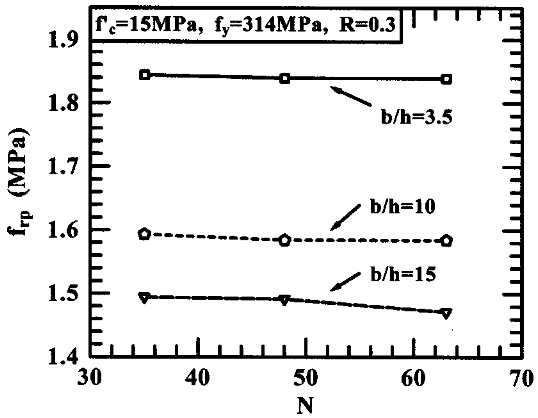

Fig. 8 Effects of element division

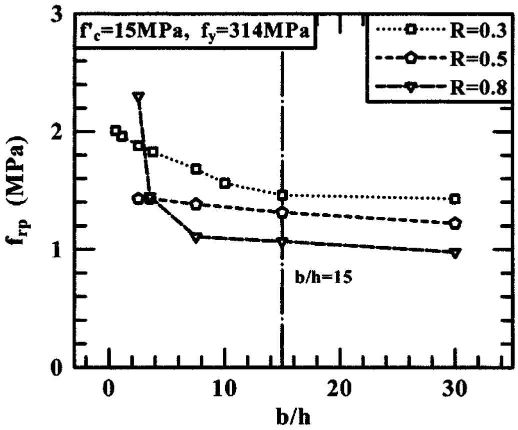

Fig. 9 Effects of *b/h* ratio

changing the height *h* while keeping the same number of elements per layer (i.e., $N = 63$). Three cases for different *R* values are examined and the maximum average lateral pressure variation against the *b/h* ratio is plotted as shown in Fig. 9. A value of 15 is selected as an appropriate *b/h* ratio for the model.

3.2. Numerical results: Square-shaped sections

The analyses are performed for 36 cases covering a wide range of material and geometrical properties as shown in Table 2. A representation of gap element distribution across a section is shown in Fig. 10. Here, F_1 represents the gap element force in an element at the center of one side and F_8 is at a corner. A

Table 2 Geometrical and material properties of square-shaped columns

f_c' (MPa)	f_y (MPa)	R
15.0, 25.0, 35.0	235.0, 314.0, 450.0	0.3, 0.4, 0.6, 0.80

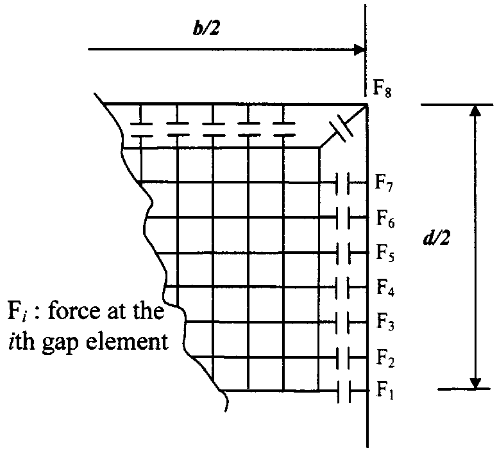

Fig. 10 Representation of gap element forces

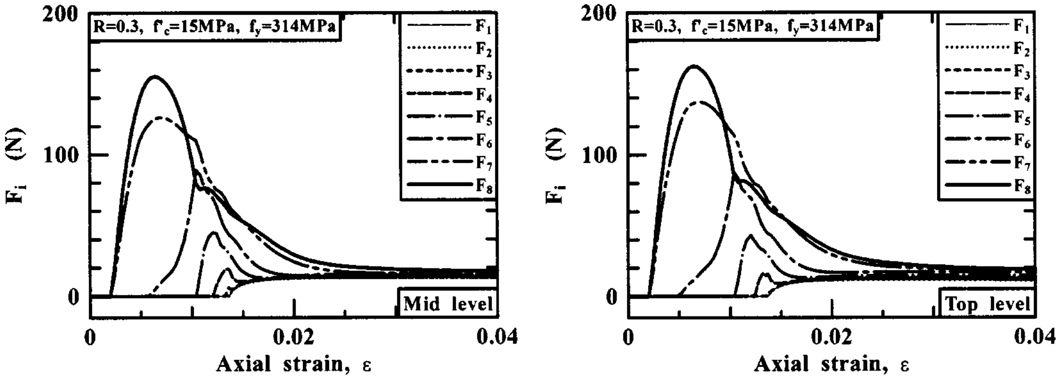

(a) at the mid level (b) at the top level

Fig. 11 Examples of gap forces across a section

representative illustration of gap element force distribution across sections at the mid and top levels are shown in Figs. 11(a) and 11(b), respectively. Since all the elements are uniformly distributed the force in each gap element can be considered as a measure of the pressure over the concrete at the vicinity of an element. It is observed that at the initial stage of loading, all the gap elements have zero forces, which means that the two materials have been separated. This is obvious because the Poisson's ratio of steel is higher than that of concrete at this stage. When axial load is increased, the Poisson's ratio of concrete is increased, and eventually it surpasses that of the steel. This leads to an excessive expansion of concrete resulting in lateral pressure developing at the concrete-steel interface. Eventually, the gaps become closed and, as a result, gap forces can be obtained. This is a well established fact that can also be verified through experimental observations. It is also interesting to note that the occurrence of gap closure is considerably delayed at the middle part of one side of the section (e.g., gap element force F_1). The corners are subjected to relatively high lateral pressures and the degree of confinement rapidly diminishes away from the corners. This was also found to be true in the case of concrete confined by lateral reinforcements, as reported by Nishiyama *et al.* (1997). Since the observed average lateral pressure difference between the two levels is insignificant, the assumption of uniform pressure distribution along the column height is acceptable.

Subsequently, the average lateral pressure, f_r, versus the axial strain of sections having different values of R, is plotted as shown in Fig. 12(a). As expected, the average lateral pressure is decreased with an increased value of R. The confinement action does not come into play until the axial strain reaches a value of about 0.002, as observed in the enlarged view of f_r at the early stage of loading (see Fig. 12(b)). The variation of lateral pressure pattern is also quite similar for all values of R.

Finally, the computed average lateral pressures from the 3D analysis and the proposed equation (i.e., Eq. (9)) are compared and presented in Fig. 13. It shows that the predictions from both the methods converge well at f_{rp} values less than about 2.0 MPa. However, beyond this limit, the deviation exceeds more than 15%. This means that the previous equation overestimates the lateral pressure when a high confinement is anticipated. By plotting the 3D analytical results against the parameter $R \cdot f_c'/f_y$ and the curves corresponding to the previous equation on one plot, the conditions producing this discrepancy can be recognized. It is understood that the difference becomes significant at higher unconfined concrete strengths, as shown in Fig. 13(b). However, it is important for practical reasons to examine the safety of predictions in terms of f'_{cc}, which is directly computed by Eq. (2) with f_{rp} values

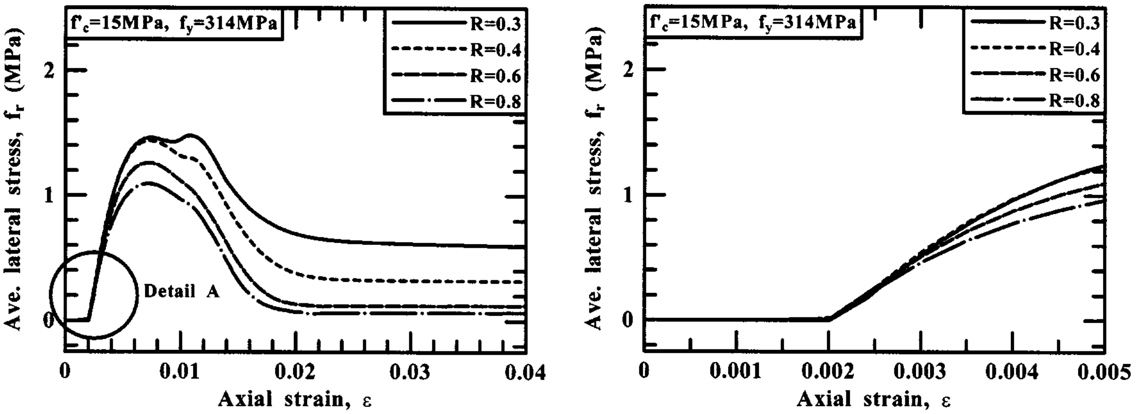

(a) Average lateral pressure for different sections (b) Detail A

Fig. 12 Example of variation of average lateral pressure

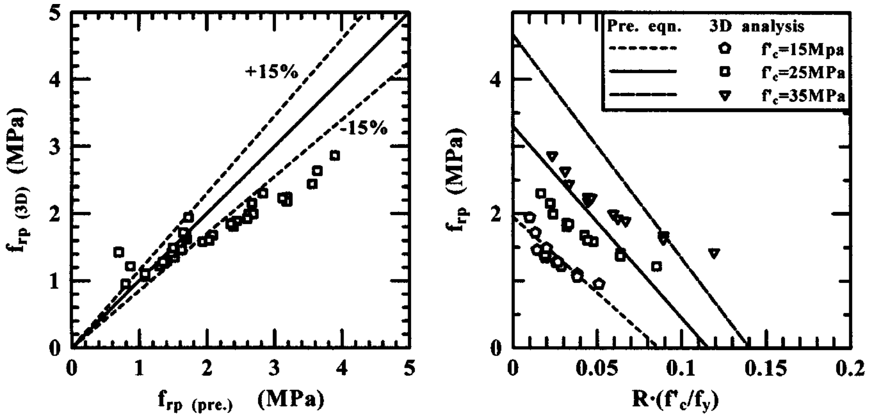

(a) $f_{rp\,(3D)}$ vs $f_{rp\,(pre)}$ (b) f_{rp} vs $R \cdot f'_c / f_y$

Fig. 13 Comparison of maximum average lateral pressure obtained using 3D analysis and previous equation

obtained through both methods. Such a comparison, as presented in Fig. 14, reveals that the previously proposed equation (i.e., Eq. 9) and the 3D analysis yield almost the same confined concrete strength predictions. This means that the simple 2D analysis method involving concrete-steel interaction model can be confidently used for practical design purposes.

3.3. Numerical results: Rectangular-shaped sections

A similar type of analytical model as adopted in the square-shaped sections is also used for the rectangular section. The *b/d* ratio is varied from 1.0 to 1.75 by keeping the length *b* constant and varying the length of shorter side *d*. Similarly for the square-shaped sections, a constant value of 15.0 is maintained as the *b/h* ratio. Then, the analyses are conducted for several cases whose material and geometrical properties are presented in Table 3. Subsequently, the average lateral pressure at each side

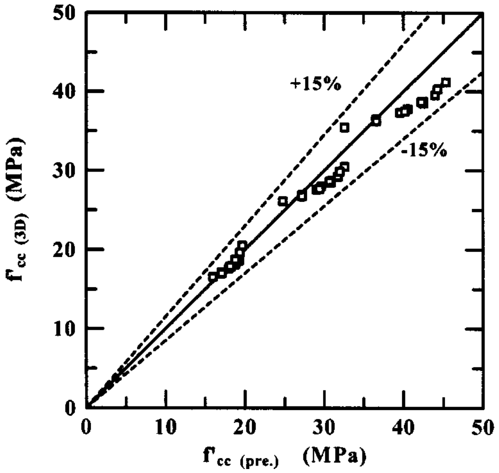

Fig. 14 Comparison of f'_{cc} computed from 3D analysis and previous equation

Table 3 Geometrical and material properties of rectangular shaped columns

f'_c (MPa)	f_y (MPa)	R	b/d
15.0	314.0	0.3, 0.5, 0.80	1.0, 1.25, 1.35, 1.50, 1.65, 1.75

is determined by

$$f_{r,b} = \frac{4\sum_{i=1}^{N_b} F_{bi}}{(b-t)h} \tag{14}$$

$$f_{r,d} = \frac{4\sum_{j=1}^{N_d} F_{dj}}{(b-t)h} \tag{15}$$

where $f_{r,b}$ and $f_{r,d}$ represent the average lateral pressure at the longer and shorter sides of the section, respectively. F_{bi} and F_{dj} are the ith and jth gap element forces and N_b and N_d are the total number of gap elements at each side, and the subscripts b and d denote the longer and shorter sides of the section, respectively. The maximum average lateral pressures at each side, $f_{rp,b}$ and $f_{rp,d}$ are obtained from the average pressure versus the axial strain curves plotted by using Eqs. (14) and (15), respectively. An example of the ratio ($f_{rp,d}/f_{rp,b}$) for different R values (R corresponds to the plate at the longer side of section) is illustrated in Fig. 15. The ($f_{rp,d}/f_{rp,b}$) ratio, or the difference between the maximum average lateral pressures on two sides, displays a linear relationship with the b/d ratio. The higher lateral pressure is found at the shorter side of the section. The ratio ($f_{rp,d}/f_{rp,b}$) is found to be virtually independent from the value of R of the component plate. The maximum average lateral pressure for the whole section, f_{rp}, is obtained from the combined average lateral pressures of two sides as:

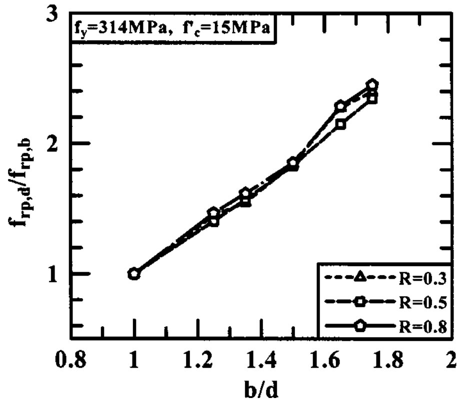

Fig. 15 Ratio of maximum average lateral pressures on sides of rectangular sections

$$f_r = \frac{4\sum_{i=1}^{N_b} F_{bj} + 4\sum_{j=1}^{N_d} F_{dj}}{[(b-t)h+(d-t)h]} \tag{16}$$

The maximum average lateral pressure of rectangular sections, $f_{rp,r}$ is non-dimensionalized by the pressure corresponding to the square-shaped section, $f_{rp,s}$ and is plotted against the *b/d* ratio as illustrated in Fig. 16(a). It is understood here that the maximum average lateral pressure increases with an increasing *b/d* ratio. Nevertheless, the maximum deviation from the values corresponding to a square-shaped section is less than 10% in the range of the *b/d* concerned. The lateral pressure obtained from the present method can then be compared with the value obtained using the previous equation (i.e., Eq. 9), with the parameter *R* corresponding to the longer side of the section. This assumption implies that when a rectangular-shaped section is concerned, the proposed equation treats it as a square

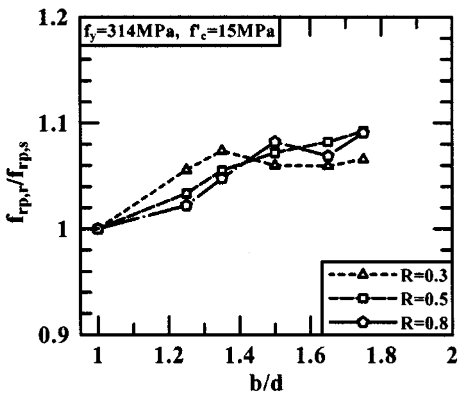

(a) Computed maximum average lateral pressures of different rectangular sections

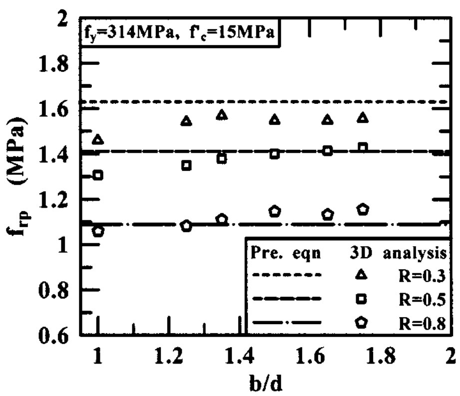

(b) Comparisons between computed and predicted maximum average lateral pressures

Fig. 16 Effects of *b/d* ratio on confinement section with sectional dimensions equal to the longer side of the rectangular section. This is a rough assumption and needs to be verified. To this end, comparisons are made between the lateral pressure computed from the present analysis and values obtained from Eq. (9), as shown in Fig. 16(b). These reveal that the previously assumed criterion for R to be used in rectangular-shaped sections is quite satisfactory. Finally, in the absence of well-established expressions for dealing with the effects of breadth-to-width ratio on the confinement at peak load, the expressions proposed for square sections should be conservatively adopted, as was the case in this present study.

4. Conclusions

This paper presented an evaluation of the maximum average lateral pressure that can be effectively utilized to estimate the confined concrete strength of CFT columns. An analytical model was proposed for the lateral pressure evaluation of box-shaped CFT columns. A three-dimensional finite element analysis procedure was used for this purpose. Based on the present numerical results and the comparisons with those obtained from the previously proposed empirical expression, the following conclusions can be drawn:

1. Maximum average lateral pressures obtained from the 3D analysis and the previously employed equation are quite close at relatively low maximum average lateral pressure values. In the predictions for higher maximum average lateral pressures, the differences between two methods tend to increase (i.e., the 3D analysis yields lower values of lateral pressures). The relatively high strength concrete resulted in higher lateral pressures with the results that the predictions for such situations using the previous equation are considerably overestimated.
2. Comparisons of confined concrete strengths computed using maximum lateral pressure obtained from both methods show that the differences observed in the lateral pressures predictions have not seriously affected the compressive strength improvement of concrete. This means that the previous simplified method is quite satisfactory in terms of strength evaluations of confined concrete.
3. Lateral pressure on the shorter side of a rectangular section is higher than that on the longer side. The ratio of the average lateral pressure on shorter and longer sides of a rectangular section seems to be proportional to the corresponding side length ratio.
4. The maximum average lateral pressure on a rectangular-shaped section is higher than that of the square section with the dimensions given by the longer side of the rectangular section.
5. In the absence of precise evaluation methods, the maximum average lateral pressure on the rectangular-shaped sections may be obtained from the equation proposed by the interaction model with the width-to-thickness ratio parameter given by the longer side of the section.

Finally, it can be concluded that the 3D analysis method as presented in this study is useful in confinement evaluations of box-shaped sections. Such evaluations can ultimately be used in confined concrete strength predictions.

References

Assa, B, Nishiyama, M. and Watanabe, F. (2001), “New approach for modeling confined concrete. II: Rectangular columns”, *J. Struct. Engrg.*, ASCE, **127**(7), 751-757.

ABAQUS/Standards User’s and Theory Manuals (1998), Hibbitt, Karlsson, and Sorensen, Inc., U.S.A.

Baba, T., Inai, E., Kai, M., Noguchi, T. and Mukai, A. (1995), "Structural behaviour of concrete filled steel tubular columns under axial compressive load, Part 2, Test Results on Rectangular Columns", In: *Abstracts of the Annual Convention of the Architectural Institute of Japan*, 737-738 (in Japanese).

Brauns, J. (1999), "Analysis of stress state in concrete-filled steel columns", *J. Constr. Steel Res.*, **49**, 189-196.

El-Tawil, S. and Deierlein, G.G. (1999), "Strength and ductility of concrete encased composite columns", *J. Struct. Engrg.*, ASCE, **125**(9), 1009-1019.

Gardner, N.J. and Jacobson, E.R. (1967), "Structural behavior of concrete filled steel tubes." *ACI Journal*, No. 64-38, 404-413.

Ge, H.B. and Usami, T. (1992), "Strength of concrete-filled thin-walled steel box columns :Experiment", *J. Struct. Engrg.*, ASCE, **118**(11), 3036-3054.

Ge, H.B. and Usami, T. (1994), "Strength analysis of concrete filled thin-walled steel box columns", *J. Constr. Steel Res.*, **30**, 259-281.

Han, L.H., Zhao, X.L. and Tao, Z. (2001), "Tests and mechanics model for concrete-filled SHS stub columns, columns and beam-columns", *Steel and Composite Structures*, **1**(1), 51-74.

Kent, D.C. and Park, R. (1971), "Flexural members with confined concrete", *J. of Struct. Div., American Society of Civil Engineers*, ASCE, **97**, No. ST7, 1969-1989.

Kvedaras, A.K. and Sapalas, A. (1999), "Research and practice of concrete-filled steel tubes in Lithuania", *J. Constr. Steel Res.*, **49**, 197-212.

Nishiyama, M., Assa, B.B. and Watanabe, F. (1997), "Prediction of stress-strain curve for confined concrete based on transverse steel-concrete interaction", *Proceedings of the Japan Concrete Institute*, **19**(2), 543-548.

Schneider, S.P. (1998), "Axially loaded concrete-filled steel tubes", *J. Struct. Engrg.*, ASCE, **124**(10), 1125-1138.

Sugupta, D.P.G. and Mendis, P.A. (1995), "Design of high-strength-concrete-filled tube column", *Proc of the Fifth East-Asia-Pacific Conf. on Struct Eng. Const.*, Griffith University, Australia, 427-432.

Susantha, K.A.S., Ge, H.B. and Usami, T. (2001), "Uniaxial stress-strain relationship of concrete confined by various shaped steel tubes", *Eng. Struct.*, **23**(10), 1331-1347.

Tang, J., Hino, S., Kuroda, I. and Ohta, T. (1996), "Modeling of stress-strain relationships for steel and concrete in concrete filled circular steel tubular columns", *Steel Construction Engineering*, JSSC, **3**(11), 35-46 (in Japanese).

Tomii, M., Yoshimura, K. and Morishita, Y. (1977), "Experimental studies on concrete filled steel tubular stub columns under concentric loading", *Int. Colloquium on Stability of Structures under Static and Dynamic Loads*, Washington, DC, 718-741.

Tomii, M. and Sakino, K. (1979a), "elasto-plastic behaviour of concrete filled square steel tubular beam-columns", *Transaction of Architectural Institute of Japan*, **280**, 111-120.

Tomii, M. and Sakino, K. (1979b), "Experimental studies on the ultimate moment of concrete filled square steel tubular beam-columns", *Transaction of Architectural Institute of Japan*, No. 275, 55-63.

Tomii, M., Sakino, K. and Xiao, Y. (1988), "Triaxial compressive behaviour of concrete confined in circular steel tube", *Transaction of the Japan Concrete Institute*, No. 280, 369-376.

Usami, T. and Ge, H.B. (1998), "Cyclic behaviour of thin-walled steel structures-Numerical analysis", *Thin Walled Structures*, **32**(1/3), 41-80.

Watanabe, H., Sakimoto, T., Senba, K. and Onishi, S. (1997), "A simplified analysis for the ultimate strength and behaviour of concrete-filled steel tubular structures", *Proceeding of the Fifth International Colloquium on Stability and Ductility of Steel Structures*, Japan, 893-900.

CC